TRANSIENT IN OPERATIONS: FROM JET-FUEL TO HYDROGEN-POWERED AIRCRAFT

Gabriele Sirtori[1] & Lorenzo Trainelli[1]

[1]Department of Aerospace Science and Technology, Politecnico di Milano, Via G. La Masa 34, 20156 Milan, Italy,
Corresponding author: gabriele.sirtori@polimi.it

Abstract

The work shown here has the ambition to assess the transition of a short-haul airliner fleet from jet-fuel to hydrogen propulsion, considering the constraint arising from the distribution of hydrogen refueling infrastructures across airports and the different performance (energetic, environmental and economic) of the two sub-fleets. The aircraft assignment to each route is performed with the objective of minimizing either the energy, the carbon intensity or the fuel cost of the overall network, obtaining different route assignment distributions. The results show that the aviation-induced temperature change can be reduced by up to 57% compared to an all-jet-fuel fleet.

Keywords: Hydrogen tankering, hydrogen-powered aircraft, fleet transition, climate impact

1. Introduction

Environmental sustainability is the big challenge that commercial aviation is facing and will be facing in the next decades. Aviation accounts for about 2% of man-made greenhouse emissions and for 12% of transport-related emissions [1]. A technological revolution is necessary, to allow the sector to comply with the Paris Agreement requirements by 2050. In this context, hydrogen is deemed as one of the best solutions to decarbonize air transport, specifically for short [2, 3] and long-range aircraft [4, 5], which would use hydrogen via direct combustion. Regional aircraft could also use hydrogen recurring to hybrid-electric architectures, in which hydrogen would be used by fuel cells to be converted into electricity [6]; this aircraft category could also recur to thermal hybrid-electric configurations, which could come to market sooner because of a higher TRL [6]. Besides research projects, there is also an emerging industrial interest in hydrogen-powered commercial aviation, such as Airbus ZeroE [7], for larger aircraft, and Zero Avia [8], for regional solutions. Such novel aircraft will need to account for the switch to hydrogen from the preliminary sizing phase, which significantly impacts the aircraft design. In fact, the bulky cryogenic hydrogen tank is placed at the back of the fuselage, requiring either a cabin shortening or a fuselage elongation. The latter solution, which allows the number of passengers to remain unchanged, causes an increase in the wetted surface and thus the required thrust. This shows the necessity of assessing the design range, one of the most important TLARs for preliminary aircraft design, to have an aircraft that is rightly sized for its mission, given the strong coupling between the design range, hence the tank size, and the aircraft performance.

The design range definition can only come from a network analysis that also accounts for the expected availability and price of hydrogen at the served airports. In fact, it is necessary to evaluate how many routes of the existing network can be served by hydrogen aircraft, eventually recurring to tankering to fly to destinations close to the reference airport with no hydrogen available. Such an analysis can be based on aircraft with different design ranges, to assess the impact on the amount of flyable routes. This analysis can be coupled with a fleet replacement model that introduces the transient from a fully kerosene-based fleet to an increasingly hydrogen-powered one. Since, especially

initially, the hydrogen fleet will not be big enough to fly all of the routes that it can potentially serve, it is possible to introduce an optimizer that assigns each city pair to either a kerosene or hydrogen aircraft, respecting the fleet ratio, with the objective of minimizing various indicators, as the overall network energy efficiency, CO_2 intensity or energy cost.
Chapter 2 briefly describes the methodology that enables assessing whether a city pair can be flown or not by a hydrogen aircraft, depending on the considered hydrogen distribution scenario. Chapter 3 presents the optimizer, the considered figures of merit and the model used to evaluate the average temperature response over an aircraft life cycle, considering the fleet transition from jet fuel to hydrogen. Chapter 4 presents the results of this analysis.

2. Sensitivity of design range of hydrogen-powered aircraft on network coverage

2.1 Methodology

As more broadly described in [9], given a network of flights from a reference airport equipped with a hydrogen refueling infrastructure, there are five possible operational cases, which depend on the presence of hydrogen refueling infrastructure at the destination airport and on the design range of the aircraft that operates that particular flight. A short route is here defined as a route whose covered distance is less than half of the aircraft's operational range ($R_{Op}/2$), meaning that the tank has enough capacity to contain hydrogen for both the outbound and inbound flights, with enough capacity for the regulatory reserves for both flights. The five route types are presented in fig. 1, depending on flight distance and availability of hydrogen at the destination. Flights of categories 1 and 3 can be

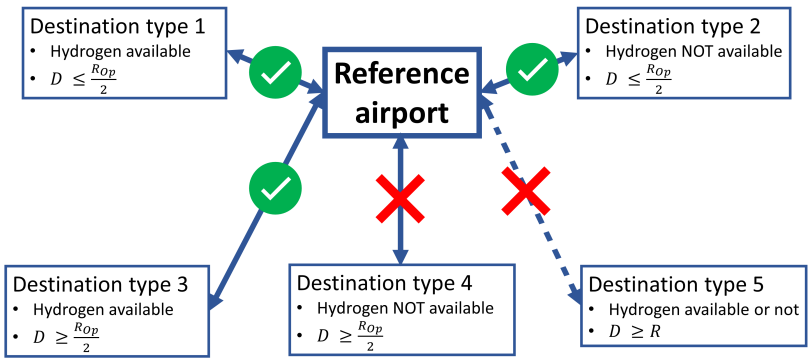

Figure 1 – Representation of operational scenarios.

operated, eventually recurring to tankering if economically interesting. Routes of type 2 can only be operated with full tankering for the return flight as the destination airport does not have hydrogen. It is necessary to remark that routes of type 4 cannot be operated by the selected aircraft, as it cannot be refueled at the destination to operate the return flight. Instead, routes of type 5 are impacted by the reduction of the design range, which will prevent the operation of certain flights, whether the destination airport has hydrogen infrastructure or not.

The optimization aims to minimize the total energy procurement cost, while assigning to each city pair its route category, assuming that the hydrogen fleet size is not constraining. The cost C is given by

$$C = \sum_{i=1}^{N} (C_{H2,Origin} F_{Origin} + C_{H2,Dest} F_{Dest})_i. \tag{1}$$

The optimizer accounts for the tank size constraint, for the aircraft performance and for the non-linearity due to an increased initial fuel load in case of tankering, thanks to lookup tables that allow computing the fuel consumption as a function of tank level and flight distance. The considered scenarios include all the short and medium-haul flights of the selected test cases. For simplicity, all the flights are considered to be operated by an aircraft based on the Airbus A320, for which several versions with different design ranges have been modeled with the in-house preliminary design methodology, HYPERION [10]. All of the TLARs, except the design range, have been left unchanged

compared to those of the A320. Some relevant information about the resulting aircraft is shown in table 1. The design range changed from the original 3,770 km to 4,000 km, 3,000 km and 2,000 km. A further version has a design range of 2,450 km, which corresponds to the maximum round trip range of 981 km, representing the average stage length for European flights in 2020, as pointed out by Eurocontrol [11].

Aircraft	Real TLARs	DR4000	DR3000	DR2450	DR2000
Design Range [km]	3,770	4,000	3,000	2,450	2,000
Max RT Range [km]	1,650	1,720	1,250	981	760
Tank capacity [kg]	5,726	6,131	4,512	3,706	3,074
Reserve hydrogen* [%]	9.5	9.0	11.9	14.2	17.0

* Reserve including 150 km to alternate airport and 30 minutes of loiter.

Table 1 – Data for aircraft with modified DR.

The hydrogen pricing model for the different airports used in this work is explained in detail in both [12, 13]. The first paper thoroughly analyses ways of supplying hydrogen to airports, namely on-site production, considering various energy sources, and off-site production, with transport via LH2 or GH2 pipelines. The on-site production was identified as the most convenient at least for larger airports, validating the approach and results of AHRES, presented in previous work of the research group [14]. The second paper lists airports and relative expected hydrogen prices and supply methods. The short- and medium-haul destinations out of Milan Malpensa are shown in fig. 2: the circles represent airports that are equipped with a hydrogen infrastructure according to [13], with the color representing the price of 1 kg of hydrogen, spanning between 1.97 €/kg and 2.97 €/kg; the black asterisks represent the destinations that are not expected to have hydrogen available. A more con-

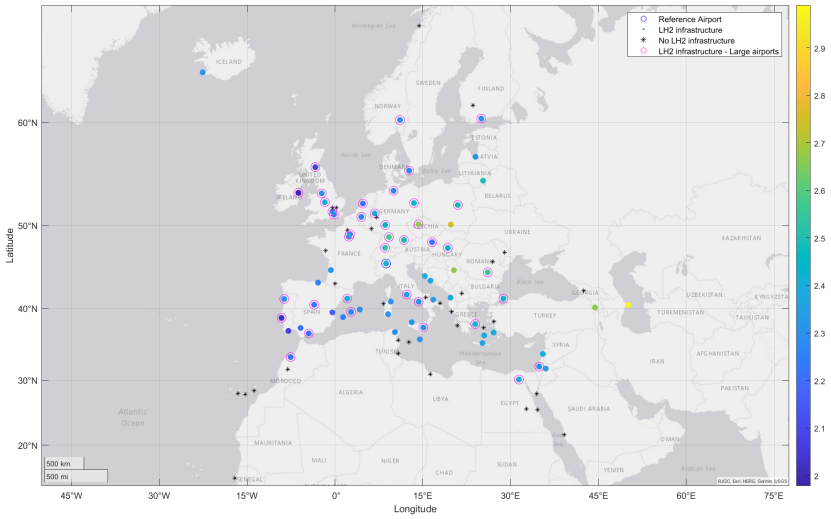

Figure 2 – Hydrogen infrastructure availability and price for the short-medium range network out of Milan Malpensa.

servative hydrogen distribution scenario has also been analyzed, considering only the airports with more than 10M passengers in 2019, marked by pink circles in fig. 2.

2.2 Results

The methodology applied to the following scenarios: Milan Malpensa (schedule of 8/09/2023, 260 flights), Amsterdam Schipol (schedule of 05/10/2023, 566 flights), Paris Charles de Gaulle (23/08/2023, 473 flights) and a more decentralized airport such as Lisbon (17/05/2024, 223 flights). Furthermore, the SAS network out of their three main hubs (Copenhagen, Oslo and Stockholm, 30/09/2024 with 324 flights) and the easyJet schedule out of Paris, London, Milan, Berlin and Amsterdam (30/09/2024

with 539 flights) have been assessed, because of a mainly domestic, thus with short routes, network and public interest in hydrogen aircraft [15] respectively.
The Milan Malpensa case has been simulated considering the Airbus A320-like hydrogen aircraft with the original design range and with four other design ranges. Furthermore, the 2,450-km aircraft has also been deployed on the more conservative hydrogen availability scenario, with the fuel being available only at large airports. The resulting route categorization for each assessed scenario is presented in fig. 3. Routes in yellow (dark and light) are the ones that cannot be operated given the particular coupling of aircraft performance and hydrogen distribution scenarios.

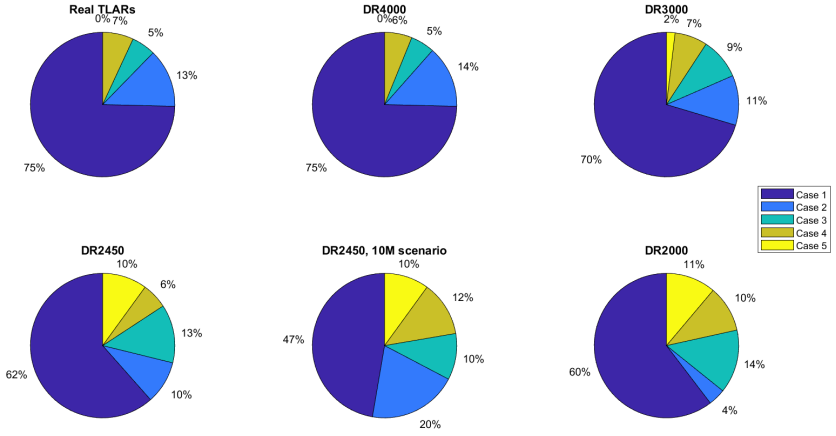

Figure 3 – Route categorization at Milan Malpensa with aircraft with different design ranges.

The reduction of the design range to 2,450 km makes 16% of flights inoperable, compared to 7% based on the aircraft with the original design range, equally achieving a 5.3% reduction in overall hydrogen mass and cost. For this reason, the other network scenarios are analyzed with this aircraft.

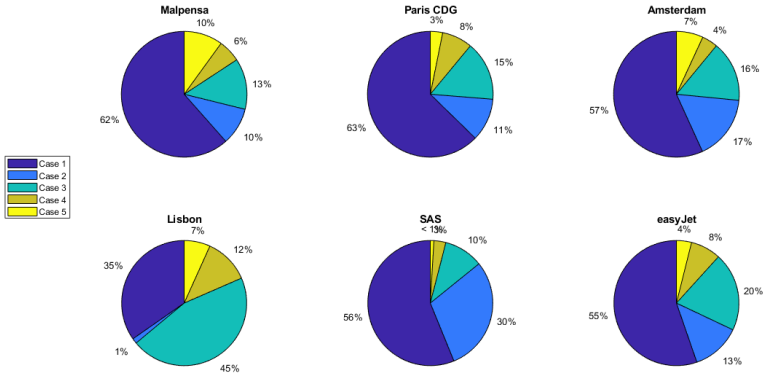

Figure 4 – Route categorization at various airports with aircraft with a 2450-km design range.

Each pie chart of fig. 4 provides insight into the feasibility of transitioning to hydrogen-powered flights by highlighting the proportion of routes (Case 4 and Case 5) requiring conventional fuel solutions or other adjustments, in each airport or airline scenario.

3. Fleet replacement and optimal route assignment

3.1 Fleet transition optimization

The preceding analysis identifies routes that could potentially be served by hydrogen-powered aircraft. However, transitioning from an entirely kerosene-based fleet to one partially powered by hydrogen will require time, as the typical lifespan of an aircraft is approximately 25 years, with hundreds of

new jet-fuel planes being still delivered every year, resulting in a gradual adoption of newer technologies. The projected share of hydrogen-powered aircraft over time, based on the fleet replacement model developed by [16], is depicted in fig. 5. The introduction of hydrogen-powered aircraft is anticipated to commence in 2035, aligning with the expected entry-into-service (EIS) date of Airbus' ZeroE project. The model has been adapted to have a maximum of 77% of hydrogen aircraft in the fleet

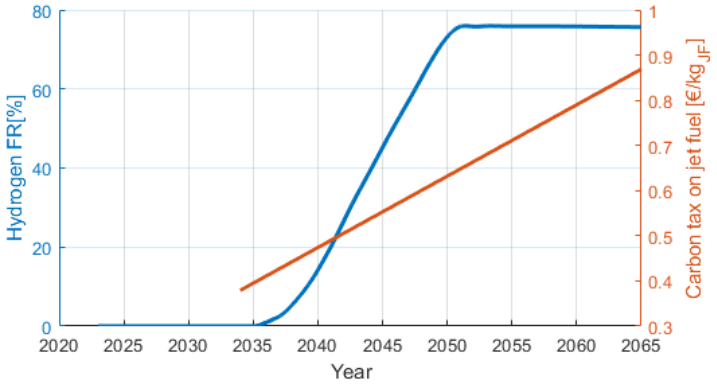

Figure 5 – Fleet ratio (FR) of hydrogen aircraft in fleet and carbon tax on jet fuel as a function of time.

to have a margin with the worst-case scenario of routes that can be operated by hydrogen aircraft, see section 2. The gradual phase-in strategy accounts for factors such as production capacity, infrastructure development for hydrogen refueling, and regulatory approvals, all essential in supporting a large-scale transition to hydrogen-powered aviation.
Integrating the previous results with the fleet replacement model enables modeling the fleet transition over a specified time frame. Since more routes and corresponding flight hours will be suitable for hydrogen aircraft than available hydrogen-powered planes, an optimization framework can be established to assign each route to either a jet-fuel or hydrogen aircraft, year to year as the hydrogen fleet ratio grows. This optimization can target one of three objectives:

1. minimize the fuel expenses of the network, measured by the Fuel Cost per Available Seat Kilometer (FCASK);
2. minimize the overall energy intensity of the network;
3. minimize the total CO_2 intensity of the network.

This optimization problem lies in the category of operations research for scheduling, which can be solved recurring to the linear integer programming methodology, such as the one used in [17]. Such optimization is crucial for operations-intense businesses such as airlines, as it provides many opportunities for efficiency, given a fixed set of assets, the fleet and the targeted network [18]. The optimization aims to minimize one of the targeted indicators, as follows:

$$minimize \sum_{i=1}^{N_{Flights}} (x_i \cdot P_{H2,i} + (1 - x_i) \cdot P_{JF,i}), \tag{2}$$

where x_i equals 1 if the i^{th} flight is assigned to a hydrogen-powered flight or 0 if the operating aircraft is kerosene-powered. $P_{H2,i}$ and $P_{JF,i}$ represent the target parameter of the optimization (cost, energy intensity or CO_2 intensity) for the i flight for the two fleets. The cost model includes the energy acquisition cost (for jet fuel, fixed at 0.816 €/kg, and for hydrogen, based on the geographical scenario presented in section 2). Furthermore, there is a linear tax on carbon emissions, hereon indicated as carbon tax (CT) spanning from 125 €/t_{CO2} in 2035 to 275 €/t_{CO2} in 2065 [19], shown in fig. 5. This basic cost model does not account for the evolution of prices, which cannot be evaluated proficiently as it depends on many external factors, such as policies, geopolitical crises and several other external factors. Furthermore, other operating costs, such as crew wages, and aircraft acquisition costs are not considered.

The proposed solving strategy does not aim to develop a precise schedule-fleet assignation, but rather to understand the optimal assignment of routes. Thus, the only imposed constraint, changing for every year of the transition, aims to guarantee that the hydrogen fleet operates the portion of the schedule that is coherent with its relevance in the fleet, as follows:

$$\sum_{i=1}^{N_{Flights}} (x_i \cdot T_i) = FR \cdot \sum_{i=1}^{N_{Flights}} T_i, \tag{3}$$

where T_i represents the time for the return trip to the i^{th} destination, also considering the time required for turnarounds, and FR represents the hydrogen fleet ratio at year y, as shown in fig. 5. Therefore, each assigned flight uses some of the total flight time allocated to either the hydrogen or jet fuel fleet. Each aircraft is modeled to be operational from 6 A.M. to 10 P.M. daily, with time allocated both to flights and turnarounds. There are no constraints regarding the sequence of flights, meaning that there is no verification of the exact flight schedule to ensure a specific flight is operated by an aircraft based on its departure time and the arrival time and airport of the preceding flight operated by the same tail. Also, constraints due to time slots, which are particularly important for airline operations, especially at larger airports, are not considered either. Passenger spillover, caused by a too-small operating aircraft compared to the traffic level on a specific route, is not evaluated in this analysis, as no real data are available. For this reason, the assumption that all considered flights are operated by the Airbus A320 and by its hydrogen counterpart is not reductive, as it is expected that the impact of hydrogen on short-haul aircraft will be similar for different sizes -i.e. on different aircraft of the A320 family. Thus, the presented optimizer indicates the best set of routes to be flown by hydrogen aircraft in a given network, from a technical point of view accounting for operational constraints for novel sustainable aircraft. Overlying these results with a normal capacity-based network planner will allow us to also detail what aircraft size operates each flight, to adapt capacity to maximize the revenue.

3.2 Climate impact modeling

To assess the overall environmental benefit arising from the fleet switch, it is necessary to consider all emissions and their impact on climate change. A good metric, introduced by [20], is the Average Temperature Response (ATR), which allows the computation of the average temperature change due to the aircraft emissions in operation and impact due to those substances remaining in the atmosphere once emitted. The ATR has been computed over the 30-year transient from kerosene to hydrogen aircraft introduced in the previous paragraph. The formal methodology presented by [20] has been updated to consider a fleet composed of both hydrogen and jet fuel aircraft, with an increasing ratio of the latter, as time advances. The theoretical definition of ATR_{30} is

$$ATR_{30} = \frac{1}{30} \int_0^{\infty} \Delta T_{Sust,30}(t) \cdot w(t)\, dt, \tag{4}$$

where the function $\Delta T_{Sust,30}(t)$ is determined based on the annual emissions rates for the first 30 years of CO_2, NO_x, H_2O, soot, and sulfate, followed by zero emissions.
The climate impact is estimated considering the emission rates presented in table 2 and for Aviation Induced Cloudiness (AIC, commonly known as contrail), a radiating factor of 2.21e-02 W/(m^2NM) for jet fuel [20], reduced by 70% for hydrogen [21], is considered.

Fuel	Jet Fuel [20]	Hydrogen [21]
CO_2 [kg/kg$_{Fuel}$]	3.16	0
NO_x [kg/kg$_{Fuel}$]	2.08e-02	2.61e-03
H_2O [kg/kg$_{Fuel}$]	1.26	8.93
SO_4 [kg/kg$_{Fuel}$]	2.00e-04	0
Soot [kg/kg$_{Fuel}$]	4.00e-05	0

Table 2 – Emission indices.

A summary of the methodology proposed by [20] is presented here. First, it is necessary to compute the radiating factor RF for each species i, with different models for long-lived gases, eq. (5a), short-lived pollutants(eq. (5b), and AIC, eq. (5c), below:

$$RF_i(t) = s_i(h) \int_0^t G_i(t-\tau) \cdot E_i(\tau)\, d\tau, \qquad \text{for } i = CO_2, NO_x\text{-}O_{3L}, \tag{5a}$$

$$RF_i(t,h) = s_i(h) \left(\frac{RF_{ref}}{E_{ref}} \right)_i E_i(t), \qquad \text{for } i = H_2O, NO_x\text{-}O_{3S}, Soot, SO_4, \tag{5b}$$

$$RF_{AIC}(t,h) = s_{AIC}(h) \left(\frac{RF_{ref}}{L_{ref}} \right)_{AIC} L_i(t), \qquad \text{for } i = AIC, \tag{5c}$$

where $G_i(t-\tau)$ represents the temporal decay of the radiating factor of substance i and $s_i(h)$ is the altitude-dependent forcing factor, to account for the different climate impact of NO_x and AIC, as a function of the emission altitude. These factors have been calculated based on the average route length of each sub-fleet during the analyzed time frame, assuming a cruise altitude of 35,000 feet. $EI(t)$ represents the emission per species as a function of time, considering the emission indices of table 2. The factors in brackets represent the RF per unit of emitted species, eq. (5b), or per unit of distance, eq. (5c).

The total change of temperature as a function of time is computed by integrating the summation of the normalized RF multiplied by $G_T(t-\tau)$, which represents the two decay modes of thermal response of the Earth system to an energy perturbation, as in eq. (6). The normalized RF is obtained considering each species' efficacy parameter f_i and the RF resulting from a doubling of CO_2, RF_{2xCO_2}:

$$\Delta T(t) = \int_0^t G_T(t-\tau) \left[\sum_i \frac{f_i \cdot RF_i(\tau)}{RF_{2xCO_2}} \right] \mathrm{d}\tau \tag{6}$$

The implementation of this methodology has been verified by application to the same scenario proposed in the reference.

4. Results

4.1 Fleet transition

The results of the analysis can be expressed by the definition of the average route length assigned to jet fuel and hydrogen aircraft and the corresponding distribution. Further relevant indicators are the sub-fleet and fleet-wide CO_2 intensity, energy intensity and FCASK. In fact, these three indicators provide a good analysis of the fleet performance in terms of environmental impact, energy efficiency, and cost considering the time-dependent hydrogen fleet ratio.

The following details results for various simulations of the Milan Malpensa case; the same approach can be used for any of the other scenarios introduced in section 2. The first set of results, presented in fig. 6 details the time evolution of the four relevant parameters, in a scenario in which the design range of the hydrogen aircraft is the same as that of the reference jet-fuel aircraft. The shown results include optimization of the FCASK and energy intensity without the CT, as well as the optimum FCASK results considering the CT. The results that minimize the CO_2 intensity are very similar to those of minimum FCASK and, thus are not shown for readability. In these simulations, the only constraint limiting the novel aircraft operations is the availability of hydrogen at the destination, especially for longer routes. The optimization accounts for the intrinsic performance difference (environmental, energetic, or economic), differentiating the two sub-fleets.

For what concerns route attribution, the two scenarios without the CT show similar results, with slightly shorter routes assigned to hydrogen aircraft in the minimum energy intensity case. A more significant difference is seen if a carbon tax is introduced, which causes a reduction in the length of missions flown by jet-fuel aircraft. Reducing the average flown distance causes the legacy fleet to operate more sectors, meaning there will also be more turnaround time (half an hour per segment) attributed to the sub-fleet. Since the in-service hours of each sub-fleet are fixed at a given year, the lower the average attributed missions, the more time is spent on the ground for turn-around, meaning that the sub-fleet has a lower weight on fleet-wide indicators. The time history of CO_2 intensity shows very similar results for the three optimal solutions, with the average indicator dropping linearly as the hydrogen FR increases. For what concerns the energy intensity, the biggest difference is seen

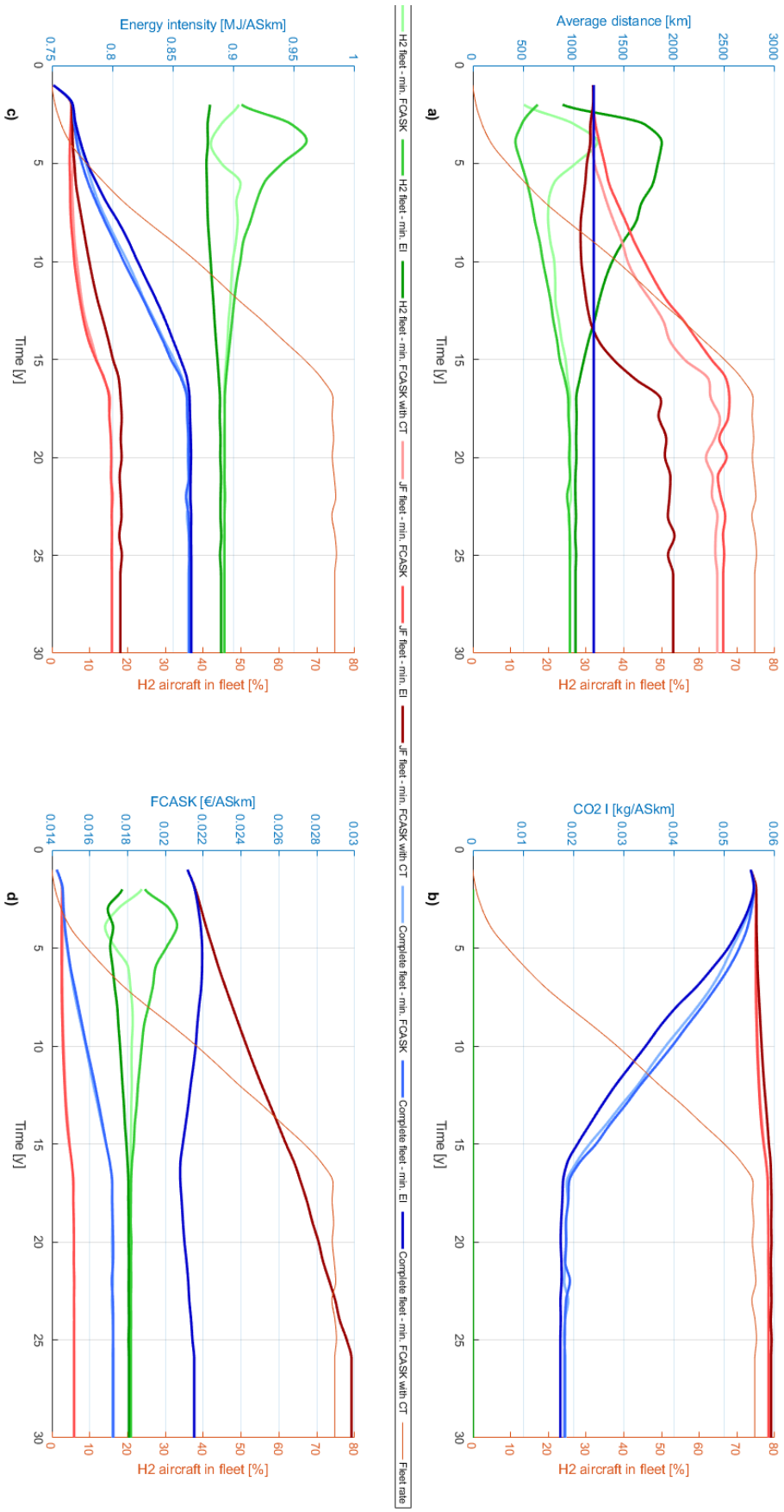

Figure 6 – Evolution for the average distance (a), CO_2 intensity (b), energy intensity (c) and FCASK (d) as a function of time, hydrogen aircraft sized with the original design range.

	Fleet ratio	Distance [km]			CO_2 intensity [kg/ASkm]			Energy intensity [MJ/ASkm]			FCASK [€/ASkm]		
		Case 1	Case 2	Case 3	Case 1	Case 2	Case 3	Case 1	Case 2	Case 3	Case 1	Case 2	Case 3
Baseline	JF 100%	1147.2			0.0552			0.7512			0.0228		
Jet fuel	75%	1075.2	1349.0	1063.3	0.0569	0.0565	0.0569	0.7744	0.7683	0.7745	0.0235	0.0233	0.0235
Hydrogen	25%	1612.3	813.8	1638.3	0.0000	0.0000	0.0000	0.8261	0.8181	0.8280	0.0164	0.0173	0.0165
Average	100%	1147.2	1147.2	1147.2	0.0417	0.0448	0.0417	0.7879	0.7788	0.7833	0.0216	0.0221	0.0216
Jet fuel	50%	1104.0	1750.1	1102.3	0.0579	0.0568	0.0579	0.7876	0.7726	0.7877	0.0254	0.0249	0.0254
Hydrogen	50%	1288.4	821.3	1286.4	0.0000	0.0000	0.0000	0.8246	0.8264	0.8252	0.0168	0.0175	0.0168
Average	100%	1147.2	1147.2	1147.2	0.0288	0.0331	0.0288	0.8062	0.7949	0.8065	0.0211	0.0218	0.0211
Jet fuel	25%	1761.6	2308.8	1765.3	0.0592	0.0585	0.0592	0.85055	0.7966	0.8049	0.0271	0.0268	0.0271
Hydrogen	75%	1039.7	951.2	1038.4	0.0000	0.0000	0.0000	0.8266	0.8289	0.8270	0.0171	0.0172	0.0171
Average	100%	1147.2	1147.2	1147.2	0.0182	0.0196	0.0182	0.8200	0.8174	0.8201	0.0202	0.0204	0.0202

Table 3 – Summary of each case on a sub-fleet and total fleet basis, considering a 25%, 50% and 75% hydrogen fleet ratio, including the progressive CT and hydrogen aircraft with a 2450-km design range. * Case 1: min. FCASK * Case 2: min. energy intensity * Case 3: min. CO_2 intensity.

during the transient, showing a higher energy intensity for the minimum cost with CT case. It is also important to point out that the average energy intensity increases by approximately 14%, because of the lower efficiency of hydrogen aircraft. The FCASK sees a 20% increase following the introduction of hydrogen aircraft for the two scenarios that do not consider the CT. In the CT Scenario instead, the FCASK remains almost constant over time, 40% higher than the initial FCASK, computed without considering the CT.

Table 3 details the results for the Milan Malpensa case, considering a 25%, 50% and 75% hydrogen fleet rate, including a CT. Differently from the results presented in fig. 6, the considered hydrogen aircraft have a design range of 2,450 km. The similarity between the solutions that minimize FCASK and CO_2 intensity is confirmed for the reduced-range hydrogen aircraft simulation. Equally, hydrogen aircraft fly shorter average segments in the minimum energy intensity solution, reducing their impact on the overall fleet performance. Furthermore, the final fleet-wide energy intensity is equal to 0.82 MJ/ASkm, compared to 0.86 MJ/ASkm in the previous case, showing the beneficial impact of the reduction of the design range of the novel aircraft. The CO_2 intensity has similar values both with the real and reduced design range hydrogen fleet. For the FCASK, the two scenarios are not comparable as the hypotheses on the CT are different. Nonetheless, the almost constant trend of FCASK previously shown by the third case is also confirmed here. The obtained values are comparable to the data available in the literature. In fact, Icelandair posts a FCASK of 0.022 $/ASkm [22]. The CO_2 intensity computed for the overall fleet by [23] is 0.6268 kg/ASkm for the baseline scenario, 0.5290 kg/ASkm and 0.3402 kg/ASkm for a FR, computed on the ratio of flown hours of the two sub-fleets, of 16.6% and 44.4% respectively. The energy intensity of the Airbus A320neo is equal to 0.7517 MJ/ASkm, considering a cabin of 180 passengers, with an expected 15% increase for hydrogen jet aircraft, as indicated in [24].

Figure 7 details how the routes are distributed among the two sub-fleets. As already clear from the average indicators shown in table 3, results obtained minimizing the FCASK and CO_2 intensity are very similar. In both cases, the hydrogen fleet is assigned to routes whose length is close to the maximum design range of the aircraft, whereas the minimum energy intensity solution sees the hydrogen flights taking up only short flights.

4.2 Climate impact evaluation

The climate impact of the different scenarios has been assessed using the methodology presented in section 3.2 This analysis accounts for all climate-altering emissions, including their latency in the atmosphere, allowing for a broader analysis than just direct computation of CO_2 emissions. The yearly jet fuel and hydrogen consumption, needed as input to compute the climate impact, depends on the hydrogen fleet ratio. The collected daily schedules are extrapolated to estimate yearly fuel consumption by multiplying the daily fuel and hydrogen usage by 365 and applying a corrective factor. This factor accounts for traffic seasonality and is derived from monthly movement data at the reference airports or bases of the carriers under consideration [25]. Furthermore, a yearly increase of

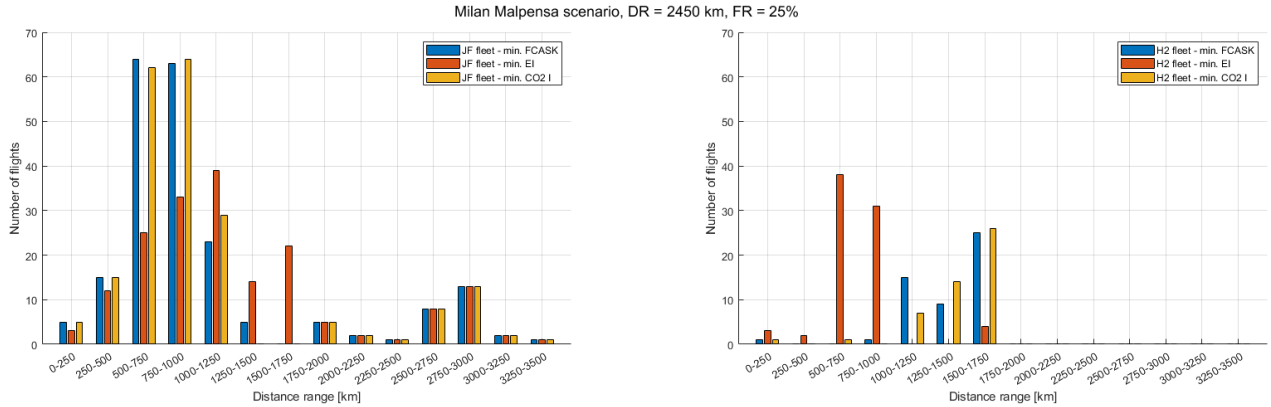

Figure 7 – Route length distribution for the 25% FR, DR2450, with CT.

traffic of 2.2% [26], assuming a fixed average stage length, is introduced, to account for the expected traffic growth and consequent emissions. The results are presented in table 4.

	Real DR						DR2450					
	No CT			CT			No CT			CT		
	1	2	3	1	2	3	1	2	3	1	2	3
ATR_{30Ref} [10^{-4}K]	2.77											
ATR_{30JF} [10^{-4}K]	1.05	1.07	0.943	0.943	1.07	0.943	1.02	1.04	0.943	0.943	1.04	0.946
ATR_{30H2} [10^{-5}K]	2.27	2.20	2.43	2.43	2.20	2.43	2.27	2.20	2.40	2.40	2.20	2.40
$ATR_{30Trans}$ [10^{-4}K]	1.27	1.30	1.19	1.19	1.30	1.19	1.24	1.27	1.18	1.18	1.26	1.19
$\Delta_{\Delta T}$ [%]	-54.1	-53.4	-57.3	-57.2	-53.4	-57.3	-55.2	-54.4	-57.4	-57.4	-54.5	-57.3

Table 4 – ATR_{30} results for the different study cases for the Milan Malpensa airport.

The results show a significant reduction of the overall climate impact evaluated as the variation of temperature measured by the ATR_{30} indicator, induced by the transitioning fleet, compared to the baseline, up to -57% depending on the case. Moreover, incorporating the CT enables a further reduction in climate impact compared to the corresponding scenario without it. The least reduction of the ATR_{30} is consistently obtained by the solutions that minimize the energy intensity, as those favor the operation of legacy jet-fuel aircraft. Conversely, the solutions for optimal FCASK And CO_2 intensity are equivalent one to the other in the simulations that include the CT, with a slight deterioration for the min. FCASK if the tax is not considered, due to a higher average CO_2 intensity of the network. It is also interesting to analyze the time history of the aviation-induced ΔT, shown in fig. 8. Plot a) shows the temperature increase linked to 30 years of operations of the jet-fuel fleet, which sees the biggest contributors being NO_x, AIC, and CO_2, which remains in the atmosphere even once operations are concluded. The peak of temperature change is at the end of the operational period, 30 years. Plot b) shows the temperature increase linked to the legacy fleet, which coupled with plot c) showing the climate impact of hydrogen aircraft, details the impact of the analyzed transient. It is interesting to notice that the shape of the total impact of the reference and of the hydrogen cases is similar, with a peak at 30 years. Instead, the progressive reduction of the jet-fuel fleet shows an interesting behavior, with a global peak at 11 years from the beginning of the operations and a local peak at the end of the 30-year period, mostly due to CO_2. At last, plot d) puts into scale the reference and the two transient scenarios, showing how positive the introduction of hydrogen aircraft is on the aviation-induced temperature increase.

5. Conclusion

The paper shows the impact of operations of a short- and medium-range fleet transitioning from jet fuel to hydrogen propulsion, considering the constraint arising from hydrogen refueling infrastructures availability and the intrinsic performance difference between the two sub-fleets. The potential routes that could be served by hydrogen aircraft, eventually recurring to tankering, are the vast majority (up to 90%, depending on the scenario). Nonetheless, there is also a strong dependence on the

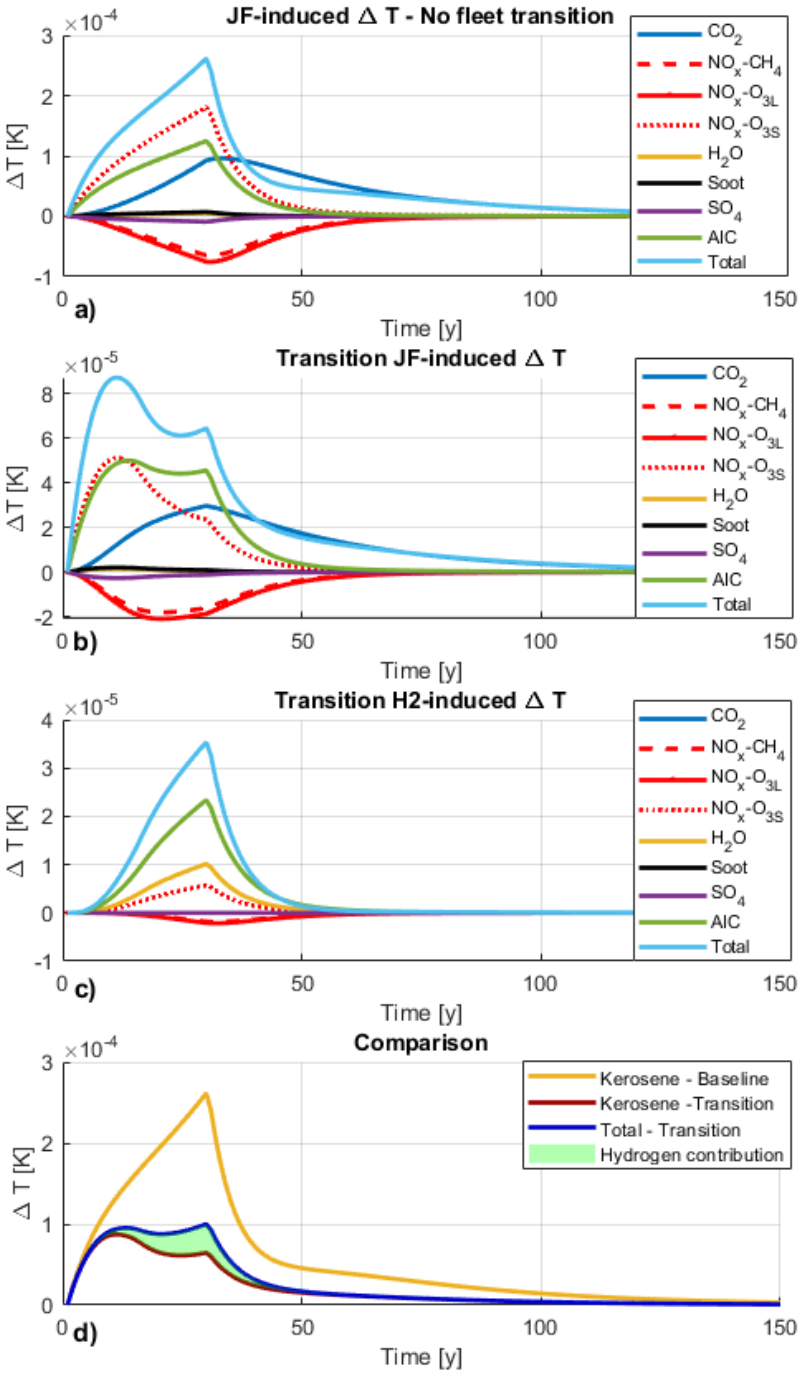

Figure 8 – ΔT response: a) Baseline scenario, b) JF impact in fleet transition c) H_2 in fleet transition and d) comparison of the three.

geographic position of the airport, as more decentralized airports can benefit less from tankering. This means that the hydrogen and jet-fuel sub-fleets can be assigned to routes, with the ambition of minimizing specific criteria, such as CO_2 or energy intensity, or FCASK. Minimum energy solutions assign the shortest routes to the hydrogen sub-fleet, whereas the other two exploit the full capabilities of the novel aircraft. The fleet transition, with hydrogen aircraft flying from 0% to 77% of the total flight hours, shows the potential of reducing the network-induced temperature increase by up to 57.4%. The presented methodology could be improved by introducing a time-evolving hydrogen refueling infrastructure scenario, in order to assess how impacting this constraint would be along the transition. Furthermore, airline data detailing passenger numbers could be included to refine the model to account for aircraft of different sizes as well.

References

[1] Air Transport Action Group. Facts and Figures. `https://www.atag.org/facts-figures/`, 2020.

[2] E.J. Adler and J.R.R.A. Martins. Hydrogen-powered aircraft: Fundamental concepts, key technologies, and environmental impacts. *Progress in Aerospace Sciences*, 2023.

[3] D. Debney, S. Beddoes, J. Darren, E. Kay, O. Kay, K. Shawki, E. Stubbs, D. Thomas, K. Weider, and R. Wilson. *Zero-carbon emission aircraft concepts*. Aerospace Technology Institute, 2022.

[4] D. Verstraete. Long range transport aircraft using hydrogen fuel. *International Journal of Hydrogen Energy*, 2013.

[5] D. Verstraete. On the energy efficiency of hydrogen-fuelled transport aircraft. *International Journal of Hydrogen Energy*, 2015.

[6] J. Eissele and S. Lafer and C. Mejía Burbano and J. Schließus and T. Wiedmann and J. Mangold and A. Strohmayer. Hydrogen-Powered Aviation—Design of a Hybrid-Electric Regional Aircraft for Entry into Service in 2040. *Aerospace*, 2023.

[7] Airbus. Zeroe: Towards the world's first zero emission aircraft, 2020.

[8] Zero Avia. The future of zero-emission, hydrogen-electric, 2024.

[9] G. Sirtori; L. Trainelli and Z. Lahmam. Hydrogen tankering: tools for economic and environmental impact scenario studies. *34th ICAS Congress*, Firenze, Italy, 2024.

[10] B. Aigner, A. Garcia Garriga, G. Sirtori, C. E. D. Riboldi, L. Trainelli, C. Mariani, and M. Mancini. Overview and preliminary results of the scalability investigation of hybrid electric concepts for next-generation aircraft (SIENA) project. In *Journal of Physics: Conference Series*, 2023.

[11] EUROCONTROL. Data snapshot: average flight distance in 2020, 2021.

[12] J. Hoelzen; M. Flohr; D. Silberhorn; J. Mangold; A. Bensmann and R. Hanke-Rauschenbach. H2-powered aviation at airports - Design and economics of LH2 refueling systems . *Energy Conversion and Management*, 2022.

[13] J. Hoelzen; D. Silberhorn; F. Schenke1; E. Stabenow; T. Zill; A. Bensmann and R. Hanke-Rauschenbach. H2-powered aviation – Optimized aircraft and green LH2 supply in air transport networks. *Preprint*, 2023.

[14] L. Trainelli; C.E.D. Riboldi and G. Sirtori. Methodologies for the Preliminary Sizing of Hydrogen-Powered Aircraft and Supporting Airport Infrastructures. *34th ICAS Congress*, Firenze, Italy, 2024.

[15] easyJet. Annual report 2022, 2023.

[16] P. Viry, T. Planès, S. Delbecq, L. Joly, and A. Salgas. An empirical and customisable fleet renewal model for prospective scenarios using open-access data. *34th ICAS Congress*, Firenze, Italy, 2024.

[17] Y. Ozdemir, H. Basligil, and B. Sarsenov. A large scale integer linear programming to the daily fleet assignment problem: A case study in turkey. *Procedia - Social and Behavioral Sciences*, 62:849–853, 2012. World Conference on Business, Economics and Management (BEM-2012), May 4–6 2012, Antalya, Turkey.

[18] C. ReVelle and A.E. McGarity. *Design and Operation of Civil and Environmental Engineering Systems*. John Wiley & Sons, August 1997.

[19] C. Valenduc. The carbon pricing proposals of the 'Fit for 55' package: An efficient and fair route to carbon neutrality. *SSRN Electronic Journal*, 2022.

[20] E. Schwartz Dallara, I.M. Kroo, and I.A. Waitz. Metric for Comparing Lifetime average Climate Impact of Aircraft. *AIAA Journal*, 49(8):1600–1613, August 2011.

[21] P. Proesmans and R. Vos. Hydrogen, medium-range airplane design optimization for minimal global warming impact. *CEAS Aeronautical Journal*, May 2024.

[22] Icelandair. Consolidated financial statements for the year 2023.

[23] N. Barry, C. Gallagher, C. Stuart, and S. Fitzgerald. Optimizing for sustainability as an objective function within airline fleet scheduling: An Ireland – EU mobility case study. 2024.

[24] D.I. Barton, C.A. Hall, and M.K. Oldfield. Design of a hydrogen aircraft for zero persistent contrails. *Aerospace*, 10(8), 2023.

[25] Aeroporti 2030. Italian airport traffic data.

[26] Eurocontrol. Forecast update 2024-2030, 2024.